Design and *in-vitro* Characterization of a Wearable Multi-Sensing System for Hydration Monitoring

Sarah Tonello, Alberto Zacchini, Alessandra Galli, Ata Golparvar, Ali Meimandi, Giacomo Peruzzi, Alessandro Pozzebon, Nicolò Lago, Andrea Cester, Giada Giorgi, Sandro Carrara, Claudio Narduzzi.

***Abstract*—Dehydration is a frequent condition in the elderly and can lead to serious health complications if not compensated timely. Early diagnosis can be problematic, as medical examinations in hospital would be needed. Fully wearable low-cost multi-sensing devices for home use could help investigate and prevent critical conditions.**

We introduce a sensing platform designed for operation in remote healthcare for the elderly. It combines a low-cost, highly customizable flexible inkjet-printed multi-sensor bracelet, including sensors for body impedance, skin hydration and temperature monitoring, with a small, low-power front-end circuit and an embedded unit that communicates by a Low Power Wide Area Network (LoRaWAN) transmission interface. We describe individual system components and present *in-vitro* experiments for their characterization. Reported results represent the fundamental proof of concept for the development of a fully operating device that can be used satisfactorily to monitor dehydration in a real-life application scenario.

***Index Terms*—Hydration monitoring; Active Aging; Inkjet Printing; Bioelectrical Impedance Analysis; *in-vitro* characterization.**

I. Introduction

Dehydration occurs whenever water balance in the human body is negative, that is, water intake is less than its output. It is a common reason why elderly patients come to emergency departments, affecting quality of life and involving a significant economic burden for the healthcare system. Moderate dehydration may cause headache, confusion, fatigue, dizziness, weakness, delirium, and high heart rate correlated with low blood pressure. If not compensated, it can develop into severe complications and eventual death [1].

Although dehydration may be occasionally assessed at home or during ambulatory visits, accurate medical evaluation involves advanced instrumentation, laboratory analyses, and specialized medical staff. In most cases it is only diagnosed when the elderly are admitted to hospital under already severe conditions. This problematic motivated researchers to focus on the development of home monitoring devices for early detection of dehydration, requiring no specialised personnel support [2]. A portable sensor that can simultaneously monitor sweat rate/loss, pH, lactate, glucose, and chloride was proposed in [3]. At specific time instants the user is required to take a photo of the sensor, that is then digitally processed to assess hydration status. However, many elders do not possess enough skill and/or physical strength to use a smartphone. In [4] a chemical sensor platform was proposed to measure potassium concentration in urine. This is only limited to urination events and not applicable to continuous monitoring. In another example the conductance of saliva is measured to assess the occurrence of dehydration, but saliva samples are easily contaminated by diet and even by simply talking [5]. All these approaches require active collaboration and some ability by the user, therefore their suitability for elderly healthcare is questionable [6].

In our work we aim at a compact, user-friendly and fully autonomous Internet of Things (IoT) based system that can reliably monitor multiple hydration-related parameters. A wireless IoT interface can be employed to relay alerts to health-care providers. The system should be wearable, non-invasive, and require no active user involvement, enabling elderly users to carry on with normal daily activities and move freely in and out of their home environment.

Following and extending our previous literature overview of existing technologies presented in [7], we propose here the design and characterization of an integrated platform that can measure physiological quantities related to body hydration using comfortable, low-cost and customized ink-jet printed electrodes and sensors. The sensor set is the result of a trade-off between medical relevance and ease of non-invasive monitoring, that led to the choice of three sensed quantities from which full hydration parameters could be estimated: body impedance and local surface impedance and local temperature.

In this paper, we introduce some linear approximations to show that relationships between the previous quantities and the global water content in the body and surface skin hydration do exist. However, such a simplified model may easily prove unsatisfactory in a practical application. Better results could be expected by inferring information about global water content and surface skin hydration through a suitable machine learning (ML) algorithm. This part will be considered in the final release of the proposed wearable system, while in this paper we focus the attention on the hardware design. The final goal of the designed sensing system is to provide early warning of impending dehydration in the elderly. For this purpose, a

Manuscript received X Month 2021.

Corresponding author's e-mail: galliale@dei.unipd.it

S. Tonello, A. Zacchini, A. Galli, G. Peruzzi, A. Pozzebon, N. Lago, A. Cester, G. Giorgi and C. Narduzzi are with Department of Information Engineering, University of Padua, I-35131 Padua, Italy.

A. Golparvar, A. Meimandi and S. Carrara are with the Bio/CMOS Interfaces Laboratory (BCI), École Polytechnique Fédérale de Lausanne (EPFL), Neuchatel, 2000, Switzerland.

This work has been supported in part by the "DEI Proactive 2018" project ("Fully printed organic array of bidirectional reference-less sensors for neuronal interfacing") and Networking project ("Smart wearable sensors for e-health applications") funded by the Department of Information Engineering, University of Padova.

simple ordinal scale related to the severity of dehydration (e.g. null, moderate, significant, severe) can suffice and accurate measurement of body water content is beyond the present scope of our work.

Results obtained from *in-vitro* characterization of each sensor are discussed in this work, as well as tests of the reliability and robustness of signal conditioning and transmission. This experimental activity is an essential prerequisite for ensuring that the prototype system will generate quality *in-vivo* data when the training database is collected. Knowledge of how each sensor responds in a controlled and standardized environment will enable to safely interpret *in-vivo* results from the multi-sensing platform and analyze them by ML-based approaches to produce the assessment of body hydration. The evaluation of variability and sensitivity of the proposed printed sensors, and the standardization of the measurement setups and protocols developed for testing and validating the printed sensors *in-vitro* aim to ensure a fair and repeatable comparison with other future sensors realized by us or other researchers.

The paper is organized as follows: preliminary considerations on hydration sensing are introduced in Section II. This is followed in Sec. III by a general overview of the system and a description of prototype design and fabrication, focusing on printed sensors, analog front-end, transmission interface and network infrastructure. Finally, Sec. IV reports on *in-vitro* sensor characterization and details the functional validation of signal conditioning electronics and transmission interface.

II. Hydration Sensing

Among the variety of measurable parameters related with hydration monitoring changes in electrical properties of the human body are the most directly correlated to fluctuation of the total body water content. Estimation by impedance analysis has been employed in several works, mostly in the form of whole-body Bioelectrical Impedance Analysis (BIA) requiring specific positioning of electrodes, such as ankle-to-ankle, wrist-to-ankle [8], or single electrodes placed on a wrist [9] or finger [10] together with a single contact placed on the opposite arm to broaden the area of body under test.

Whole-body BIA does not satisfy our requirements for unobtrusive and autonomous operation, that could be met instead by *segmental* BIA, where electrodes are placed over a small area of the body (e.g., within a bracelet), with the advantage of much reduced sizes and bulk [11]. Despite convenient in term of portability, the main problem in such miniaturized BIA systems is that shrinking the measurement on a small volume increases the significance of other physical factors such as temperature, sweat or moisture due to impaired skin transpiration under the bracelet, thus increasing the contribution of surface currents, that affect measurement as a whole and in particular the contact impedance between electrodes and skin. Interference is known to be negligible in whole-body measurements [12], but could have a more significant impact with reduced electrode size [9], the use of a non-transpiring bracelet, and above all, the far reduced volume under test. Yet, although possibly less accurate, segmental BIA is considered a useful tool for body impedance estimation [13]. In view of our aim, we decided to apply segmental BIA to the arm, exploiting multi-sensing to detect and compensate for impedance variations due to changes in temperature and superficial hydration conditions. Our design relies on a bracelet equipped with a set of printed sensors, as shown in Fig. 1. The four electrodes for tetra-polar BIA are augmented by two other sensing elements, targeting surface information of the subject skin: an inter-digitated electrode (IE) providing a sensing area for superficial hydration, and a resistance temperature detector (RTD).

The actual placement of sensors around the arm is illustrated in Fig. 2 , with a qualitative indication of relevant electromagnetic field lines. Darker outer layers in the arm cross-section represent the skin, the lighter pink part refers to body tissues, the bone being the middle white part.

Field lines going through all skin and body tissues evidence that BIA can be seen as a 3D system, whereas interdigitated electrodes cover a 2D surface portion of limited depth, which evidences their importance to help discriminate the effect of surface currents. Careful consideration must then be given to the problem of separating the contribution of body hydration from that of skin hydration when impedance is measured.

The measured body impedance can be described by different equivalent circuit models [11]. In the following, the much-simplified circuit of Fig. 3 will be employed since it satisfies completely the level of accuracy required for the analysis proposed. The circuit represents BIA current through the body by the parallel of two paths. The main path is an RC parallel that globally accounts for characteristics of the electrodes, the superficial skin layer and the deeper tissues. The undesired surface current path due to sweat and surface moisture is modelled by resistance R_{sweat}.

According to this model, the resistive part of the measured body impedance is the parallel between R_{body} , accounting for body hydration, and R_{sweat}, which accounts instead for *skin* hydration. This latter contribution once quantified will have to be compensated, since it is influenced mainly by surface sweat and humidity, which do not participate to the overall body hydration. Changes in skin electrical properties measured thanks to the IE sensor provide additional information regarding sweat rate, environmental humidity and the specific water content of the skin layers. These information will therefore complement the picture provided by BIA electrodes for a more accurate assessment of the *body* hydration status of the subject. As shown in Fig. 4, the equivalent circuit for skin impedance measurement is the series of R_{skin} and of an RC parallel modeling the contact area of the superficial skin patch.

Resistances R_{body}, R_{skin} and R_{sweat} all vary with water content, therefore their resistivity must be assumed to vary with the relative water content in the volume of interest, indicated by α. This can be indicated generically by $\rho(\alpha)$, it must be remembered that the value of α for body resistance R_{body} will in general differ from those applicable to skin resistances R_{skin} and R_{sweat}.

These simple models allow to show how resistance measurements obtained by BIA and IE can be combined to improve the estimation of overall body resistance, and obtain from that an assessment of body water content. Under the sim-

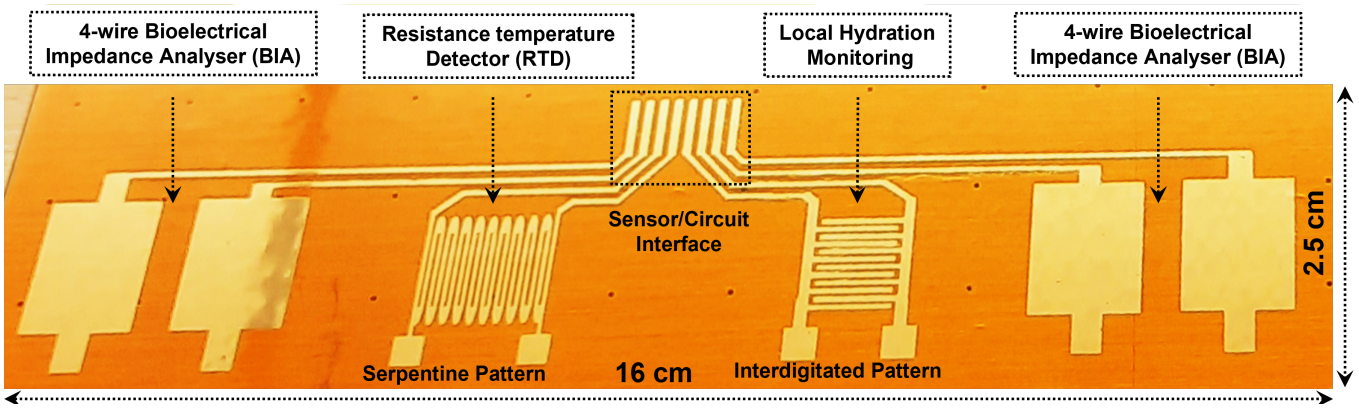

Fig. 1. Inkjet printed multi-sensing flexible bracelet with serpentine RTD, interdigitated local hydration sensors and tetra-polar BIA electrodes.

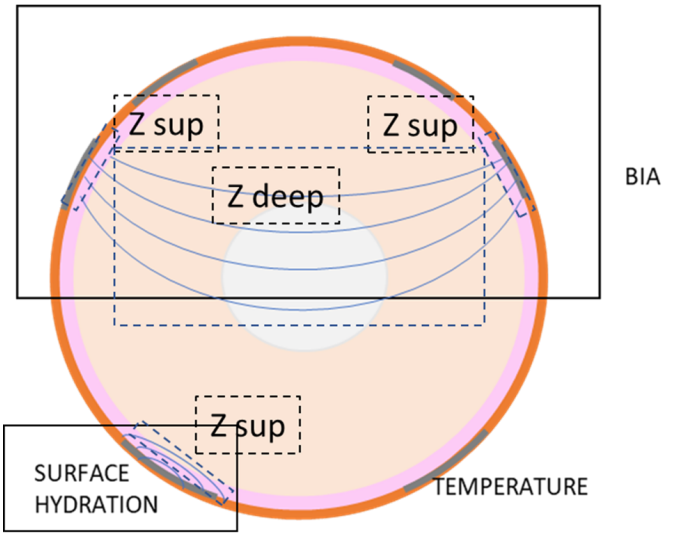

Fig. 2. Sensing with BIA electrodes and interdigitated electrodes (IE) – illustration of electromagnetic field lines in the arm cross-section. Dark outer layers represent the skin, lighter pink part refers to body tissues, while the bone is represented by the middle white part.

plifying assumption that skin resistivity is homogeneous (or considering *average* resistivity), measured skin resistance is: $R_{skin} = \rho(\alpha_{skin})(l_{IE}/S_{IE})$, where l_{IE}/S_{IE} is a geometric factor for the IE sensor.

For the total resistance R_{meas} measured by BIA, the component R_{sweat} related to skin surface current will be characterized by an average resistivity similar in value to that of R_{skin}, but in general $\alpha_{skin} \neq \alpha_{body}$ and the component R_{sweat} affects only a fraction of the BIA sensing volume. One may write:

$$R_{sweat} = \rho(\alpha_{skin}) \cdot \delta \cdot \frac{l_{BIA}}{S_{BIA}}, \tag{1}$$

where l_{BIA}/S_{BIA} is the geometric factor for the BIA sensor

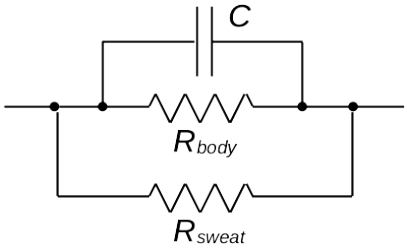

Fig. 3. Equivalent circuit model for BIA impedance.

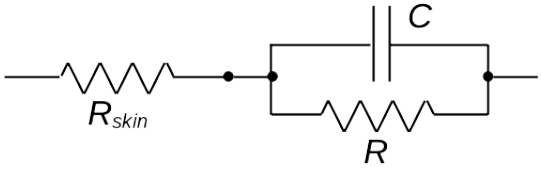

Fig. 4. Equivalent circuit model for surface impedance.

and $\delta < 1$ accounts for the fraction of the sensing volume where the contribution of sweat is significant.

To a first approximation, therefore, one has:

$$R_{sweat} = K \cdot R_{skin} \tag{2}$$

where K is a factor determined by the geometries of the two hydration sensors in the system:

$$K \cong \delta \cdot \frac{l_{BIA}/S_{BIA}}{l_{IE}/S_{IE}}. \tag{3}$$

More generally, K should be considered to account for all factors related to the sensor layout in the system.

It should be remarked that accurate calibration by this approach would only be possible if an *exact* relationship was known. This short analysis evidences that quantities of interest are indeed related, and motivates our interest in a ML-based approach for elementary-level hydration monitoring, rather than obtain R_{body} from R_{eq} and R_{sweat} via equations (2) and (5).

Finally, since temperature is related to changes in both hydration and sweat, the temperature sensor is useful as an indicator of possible effects of the ambient environment on

measured impedance values. The local temperature measured by the RTD is influenced by body core temperature, with water content acting as a thermo-regulator. Still, most of all, it depends on environmental temperature, whose variations can affect hydration and, possibly, the performances of conductive electrodes. Accurate temperature measurements serve as useful feedback when processing the other sensed quantities, to correct and interpret the results obtained. It represents essential information in a multi-parametric perspective, contributing useful data for determining the hydration status of a subject [14].

III. System Design and Fabrication

The general architecture for any wearable device typically encompasses three main sub-systems: i) sensing; ii) signal conditioning iii) data transmission, as illustrated in Fig. 5. The proposed prototype was designed and extensively tested to demonstrate its functionality as a multi-sensing device, paving the way to future miniaturization and applicability to *in-vivo* test. As illustrated in the functional diagram of Fig. 6, system hardware can be divided into seven functional blocks, three of which refer to the RTD analog read-out path.

A. Printed Sensors

Sensor geometries are designed to optimize transduction performances, allow wearability and ease of interfacing with the readout electronics. The specific choice in term of sensors, dimensions, and positioning of the device results from a combination of the measurement we want to perform (i.e. estimation of hydration level) with the specific requirements imposed by the application target (Fig. 1).

Electrodes for BIA were designed in a tetrapolar configuration, with dimensions for each electrode of 1×1 cm. Four-wire measurement enables compensation for contact resistance, thus achieving accurate results even with reduced-size electrodes, as suggested in the literature [15].

Sensors for skin hydration monitoring were designed with an interdigitated layout and a sensing area of 1 cm^2. This layout is the most sensitive to changes in the skin electrical properties (i.e., dielectric permittivity and electrical conductivity) caused by small local variations of water concentration in skin tissues.

Body temperature is sensed by a RTD contact temperature sensor. A serpentine pattern was chosen to increase the available sensing surface in a miniaturised area and obtain good sensitivity to temperature changes [16]. The geometry thus compensates for the effects of the complementary materials combined to the conductive ink to allow flexibility, that affect sensitivity as well as producing some non-linearity in the sensor response.

Inkjet printed technology was selected to fabricate all sensing elements on a flexible bracelet, that can be easily miniaturised and integrated in a wearable device. Compared to screen-printing, inkjet printing offers high-resolution patterning, improved process flexibility and prevents waste of precious material, being a mask-less drop-on-demand technique [17].

Sensors were realized by a Dimatix DMP 2850 inkjet printer (FUJIFILM Dimatix, Inc., Santa Clara, California (USA)). A polymide foil (i.e., Kapton, Dupont) with a thickness of $50\,\mu$m was chosen as substrate. Due to excellent thermal, electrical, mechanical, and chemical properties, this material represents the most suitable candidate for printed electronics applications, enabling optimal ink adhesion during printing and stability after curing [18]. Furthermore, its narrow thickness affords optimal flexibility and conformability to the skin. For all sensors a silver ink was selected (Sicrys™ I40DM-106 from PVNanocell, Israel). It is a commercial engineered conductive ink, based on single-crystal silver nanoparticles in diethylene glycol monomethyl ether (DGME), designed specifically for digital inkjet printing. After printing, all sensors were cured on a hot plate for 30 min at a temperature of $250\,^{\circ}$C, as suggested by the ink datasheet, then stored in a glove box until use.

B. Front-end Read-out Circuitry

The flexible multi-sensing element integrating BIA electrodes, IE and RTD was interfaced with a custom-designed read out front-end hardware, designed with particular attention to low-power battery operation, as well as high measurement resolution and sensitivity. Although the prototype circuit was produced on a rigid board for the development stage, the design was specifically thought for ease of miniaturization and migration to a flexible printed circuit board substrate in future works.

4-wire and 2-wire skin impedance spectroscopy are implemented by a single commercial analog front-end chip (Analog Devices AD5941), that provides a full stand-alone, self-contained measurement system, thereby vastly reducing circuit component count [19]. The chip includes an internal high-precision AC voltage source, that is employed to excite the sensors with a sinewave at known frequency, superposed to a common-mode bias voltage. The resulting current waveform, after scaling, is recorded by a 16-bit ADC, enabling to measure sensor impedance and detect its variation by the vector ratio of voltage across the unknown impedance to current flowing through it. Discrete Fourier transform calculation yields the impedance real and imaginary parts. Measured values are forwarded to the microcontroller through a serial peripheral interface (SPI) digital line.

Only a few peripheral passive components need to be added to comply with IEC 60601-1 basic safety requirements, as described in the AD5941 datasheet. A pair of capacitors and limiting series resistors, placed close to the chip at each impedance measurement port, provide DC isolation and limit the maximum allowable current into the human body.

For temperature sensing, the input low-pass analog filter stage is designed to improve common-mode rejection ratio (CMRR). Its common-mode and differential-mode bandwidths are $F_{cm} = 16\,$kHz, $F_{dm} = 1.5\,$kHz, respectively. This is followed by the 4-wire RTD sensing unit housing an instrumentation amplifier set to a gain of 1000 and a highly accurate constant RTD current source of $100 \pm 0.5\,\mu$A (Ref200, Texas Instruments, USA).

The Texas Instruments INA122 instrumentation amplifier is specifically designed for battery-powered applications with

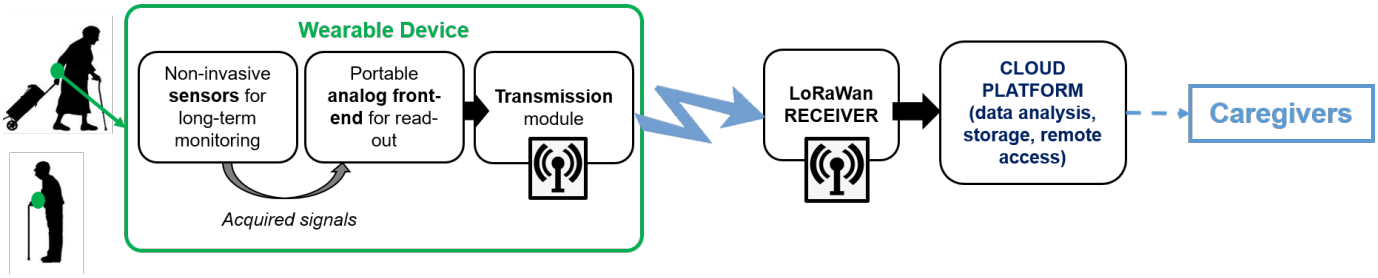

Fig. 5. Scheme representing the general system architecture of the proposed prototype.

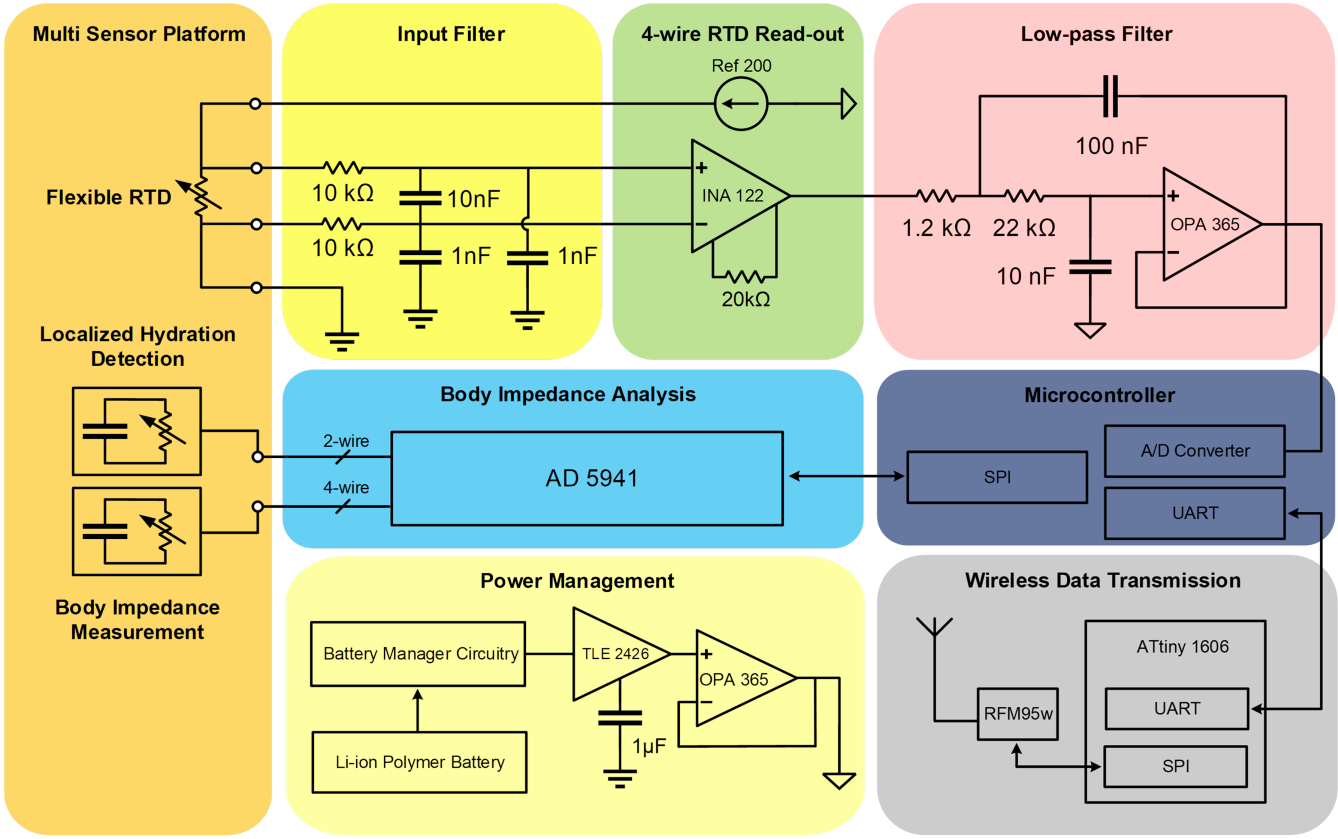

Fig. 6. Overview of the complete device architecture: hardware-level schematic for the sensor read-out front-ends; embedded processor for data acquisition and analysis; LoRaWAN wireless unit for secure low-power medical data transmission.

the capability of running on a single supply [20]. Its output is further filtered by a sharp roll-off second-order Butterworth low-pass (LP) active filter, based on Sallen–Key topology, with unit gain and cut-off frequency of 1 kHz. A Butterworth filter was preferred due to its smooth frequency response and lack of pass-band ripple, while Sallen-Key topology was preferred as it requires fewer components. This acts as an anti-aliasing filter for the microcontroller analog to digital converter (ADC) and further removes out-of-band high frequencies. The operational amplifier in the low-pass filter (Texas Instruments OPA2365) was selected due to its single-supply and rail-to-rail features. As the group delay of the entire read-out chain is negligible it directly translates RTD resistance into voltage at the input of the internal 16-bit ADC to the ST Microelectronics STM32F446 microcontroller, where the actual temperature value is computed.

All circuits are powered by a rechargeable lithium-ion/polymer battery connected to a Microchip MCP73831 single-cell charge management controller. A Texas Instruments TPS61090 DC-DC boost converter and TLE2426 ”rail splitter” were employed to provide the required supply voltage and current, with proper virtual ground termination. Additional buffers with higher current ratings were included in the power management unit as a safety margin, in particular to support the higher peak currents on the RF transceiver. Since RF bursts are very short, this will not have a significant impact on the overall consumption of the unit.

Fig. 6 shows a preliminary block diagram where two different micro-controllers (STM32F446 for data acquisition and ATtiny 1606 for data transmission) are present as a

matter of practicality. This enables to split development and characterization of different system blocks during prototype validation but, of course, a single micro-controller is more than enough, and this change will be done in the final revision of the system, leaving only the latter.

C. Data Transmission and Network Infrastructure

The transmitting interface is required to be simple, yet effective, taking into consideration all the constraints arising from the need to monitor subjects in wide areas, and the desire to avoid reliance on the active use of a mobile phone for data transmission. The latter aspect turns out to be the defining factor in the choice among IoT enabling technologies, as it emphasizes the need for long-range coverage to allow the monitoring of elderly people without hindering their mobility. Long Range (LoRa) modulation and the LoRaWAN protocol proved to be well-suited, thus being employed for the prototype. LoRaWAN was found to offer a very good trade-off between long range, low power consumption, low hardware cost, and adequate data rates for the application scenario of this work [21]. The protocol is characterised by data rates of 50 kbps at most and allows a fairly limited maximum payload size (no more than 222 B or 242 B, depending on the geographic region where the technology is deployed). Since the monitored physical quantities vary slowly over time, neither are constraining for this application scenario.

The core of the wireless data transmission interface is a Microchip ATtiny1606 microcontroller, that is connected via a SPI interface to a HopeRF RFM95w LoRaWAN transceiver. LoRaWAN allows to set up an independent, pervasive monitoring infrastructure, ensuring coverage up to some km in a single hop, by which clinicians and caregivers can remotely monitor hydration levels of patients without requiring them to manage data transmission. Provision of autonomous wireless connectivity thus removes a possible source of error/failure. The transceiver is fitted with a $\lambda/8$ whip antenna having a 2 dBi gain. Maximum current drawn during transmission is 80 mA, turning out to be adequate for battery-powered systems [22].

Digitized values measured by the three sensors are sent from the STM32F446 microcontroller to the ATtiny1606 microcontroller via a Universal Asynchronous Receiver Transmitter (UART) interface port. The three sensor readings are arranged into a LoRaWAN packet payload by the ATtiny1606 microcontroller, encrypting them by the Advanced Encryption Standard (AES)-128 exploiting two keys. The packet is then sent to a LoRaWAN gateway, employing a frequency diversity scheme via a frequency hopping technique on 8 different channels in the $863 - 870$ MHz ISM band, a Spreading Factor (SF) 7 and bandwidth of 125 kHz. The Message Queue Telemetry Transport (MQTT) protocol is employed for forwarding data via the Internet.

The gateway acts as a packet forwarder and conveys the demodulated packets, along with metadata related to reception quality indicators, to the cloud network infrastructure. The remote network infrastructure on the cloud includes an MQTT broker and a network server. It decrypts LoRaWAN packets, then stores all information related to both packet payloads, containing the sensor readings, and quality indicators, related to gateway reception, in a local database. In this way, the network can be monitored and maintained, while data are made available to users and caregivers, in particular clinicians, for the follow-up of their patients.

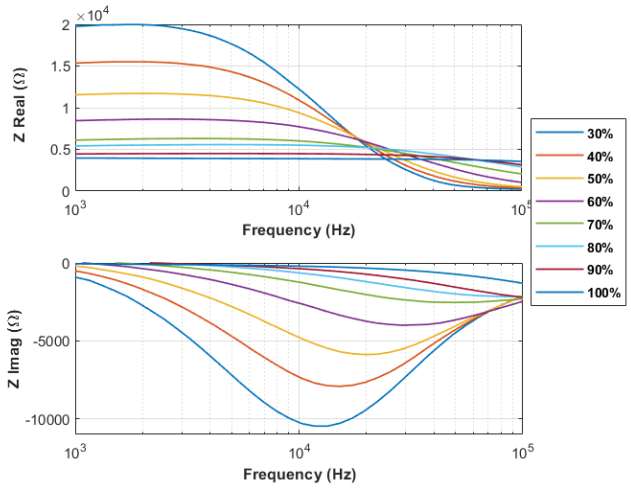

Fig. 7. Response of BIA electrodes to different hydration levels in the frequency range from 1 kHz to 100 kHz.

IV. System Characterization

A. Printed Sensor Characterization

Printed sensors were characterized *in-vitro*, in a measurable and controlled environment ensuring standardized procedures and repeatable results. Accurate bench-top instrumentation was employed to reduce measurement uncertainty and provide a reference.

Electrodes for BIA analysis were characterized exploiting a simple test structure mimicking a human arm. Electrodes printed on the polymide substrates were placed on a layer of synthetic skin-like patch wrapped around a cylindrical sponge, thus replicating the sectional layout of Fig. 3. The acquisition front-end was replaced by a bench-top impedance analyzer (Agilent E4990A, Precision LCR Meter). Different levels of volumetric water content, the typical measurement unit used to indicate hydration status, were set by injecting determined and increasing volumes of water in the sponge with a syringe. As the actual volume of the 3D setup was 10 cm^3, injection of water in a range from 3 ml to 10 ml resulted in volumetric water contents ranging from 30 to 100%.

This range of values was selected assuming the average normal ranges of hydration indicated by the clinical literature (50-65% for males and 45-60% in females) [23], so that conditions going from severe dehydration ($< 30\%$) to hyper-hydration ($> 80\%$) were represented.

Impedance at different levels of sponge hydration was measured in the frequency range between 1 kHz and 200 kHz with a 4-wire layout, like the one employed by the AD5941 analog front end.

Fig. 7 shows the real and imaginary parts of impedance (respectively, Z_{real} and Z_{imag}), plotted versus frequency as

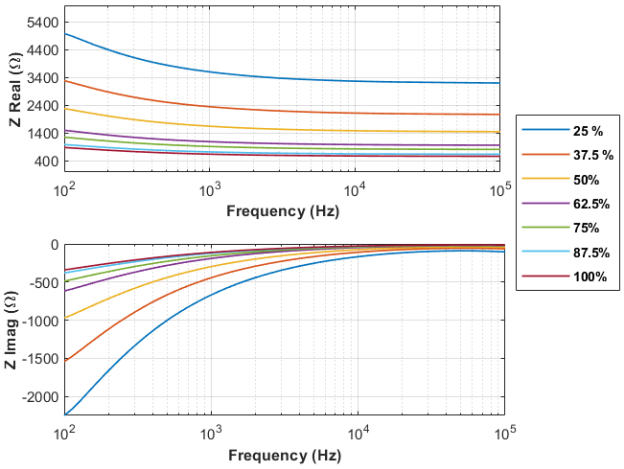

Fig. 8. Response of IE sensors to different hydration levels in the frequency range from 100 Hz to 100 kHz.

measured by the LCR meter. The instrument refers to a series impedance configuration (i. e., $Z = R + jX$), that for the circuit model of Fig. 3 has the mathematical expression:

$$R + jX = R_{eq}\left[\frac{1}{1+(\omega R_{eq}C)^2} + j\frac{\omega R_{eq}C}{1+(\omega R_{eq}C)^2}\right], \quad (4)$$

where:

$$R_{eq} = \frac{R_{body}\cdot R_{sweat}}{R_{body}+R_{sweat}}. \quad (5)$$

and C is the sensor capacitance.

Measurements agree with the assumed circuit model and show well the effect of different hydration levels on impedance. As water content increases and R_{eq} decreases accordingly, the reactance peak value occurs at progressively higher frequencies, showing that it is not advisable to refer to reactance for this kind of measurement. However, up to 1 kHz its contribution can be considered negligible (less than 5% of magnitude $|Z|$) in any hydration condition.

IE sensors for skin hydration monitoring were also characterized in a range of simulated skin hydration conditions. In this case the sensing area was placed over a layer of synthetic skin-like patch injected with controlled volumes of water, ranging from 50 μl to 200 μl.

Considering a constant volume of 200 mm^3 for the skin-like patch, a range of volumetric water contents going from 25 to 100% were tested, thus including all possible conditions that can be encountered in real scenarios including severe dehydration ($< 40\%$), mild dehydration (40 to 50%), normal skin hydration (50 to 70 %), up to hyper-hydration or edema ($> 80\%$).

Using again the Agilent E4990A Precision LCR Meter, impedance was measured in a frequency range between 100 Hz and 100 kHz, measurements being repeated for six sensor specimens. The plots presented in Fig. 8 are also in the format of an equivalent series impedance $Z = R + jX$, that for the IE equivalent model of Fig. 4 yields the formula:

$$R_{skin} + R\left[\frac{1}{1+(\omega RC)^2} + j\frac{\omega RC}{1+(\omega RC)^2}\right] \quad (6)$$

where R and C are electrical parameters of the interdigitated electrode. Results confirm the ability to discriminate different levels of hydration also in the synthetic skin-like patch. An IE sensor responds to an increase in water content by a decrease in both Z_{real} and the absolute value of Z_{imag}, as shown in Fig. 8, in agreement with the literature [24].

For Z_{real} sensitivity to hydration changes is similar throughout the range of tested frequencies, Whereas the contribution of Z_{imag} is higher at the lower frequencies (up to 1 kHz). Although electrode capacitance is significant because of the typical IE geometry, at frequencies of about 10 kHz or higher its contribution is negligible and measured impedance becomes resistive only, its value practically coinciding with R_{skin}. Figs. 7 and 8 evidence that for our purposes measurements are best taken as Z_{real} at 1 kHz for the BIA sensor and at 10 kHz for the IE sensor.

Using these plots it is also possible to compare resistances Req and R_{skin} at common uniform levels of hydration. This provides the opportunity to check our assumption in model (2) by considering ratios of $R_{body}(1kHz)$ to $R_{skin}(10kHz)$ at different hydration levels, although in this case $\delta = 1$ in (3), a condition that would hardly occur in practice. The resulting ratio is indeed nearly constant and its average value was found to be 7.8, with a standard deviation of 0.5, which is enough to confirm a proportionality relationship.

Calibration curves were built from characterization plots for Z_{real} similar to those reported in Figs. 7 and 8, obtained for four set of measurements replicated on different sensors. Extremely good results were obtained for both BIA and skin hydration IE using a single-exponential fit, as shown in Figs. 9 and 10, with a value $R^2 = 0.99$ in both cases. The two resulting equations:

$$R_{body} = 43.6e^{-0.03\alpha} \qquad \text{and:} \qquad R_{skin} = 8.9e^{-0.03\alpha},$$

show that exponential coefficients agree, whereas in this case $R_{body}/R_{skin} = 4.9$. The difference from the result above is mostly determined by the limited reproducibility of the 3D test set-up, namely, by the way the sponge and skin-like patch are assembled. This is not considered an issue, as it actually reflects the real-life situation with monitored subjects. Additional physical features will have to be included among the training inputs for an ML classifier, and these might include the arm circumference where the sensor bracelet will be located and the subject body mass index (BMI). Variability assessed for Z_{real} by a relative standard deviation (RSD) lower than 30 % in BIA and than 35 % in IE appears significant but acceptable considering the aim of our design and in agreement with RSD values shown by similar BIA analyzers [11] and by studies dealing with IE for hydration sensing [25]. This value can be explained with contribution of both sensor physical realization and setup construction.

Finally, resistance changes due to temperature ($0.04\,\Omega/°$C) within an expected temperature range $< 5°$C appear to have negligible influence compared to variations in water volume (hundreds of $\Omega/\%$).

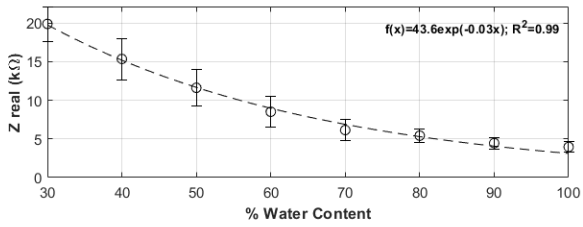

Fig. 9. Calibration of Z_{real} evaluated at 1 kHz for BIA at different volumetric water contents.

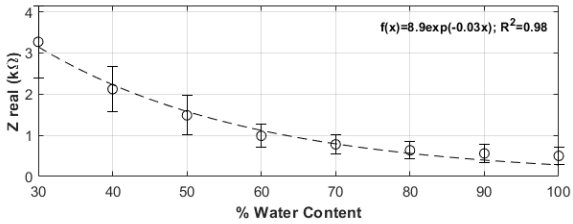

Fig. 10. Calibration of Z_{real} evaluated at 10 kHz for IE sensors at different volumetric water contents.

Temperature sensors were characterized by means of a hot plate with manual temperature control. To ensure a more homogeneous heat distribution, a layer of synthetic skin-like patch was placed between the sensor and the hot plate. The temperature on the patch surface in contact with the RTD was measured by a commercial thermometer (Hanna Instruments HI 98501 Digital Thermometer [26], accuracy $0.3\,^{\circ}$C, resolution $0.1\,^{\circ}$C). The resistance between the terminals of the serpentine RTD was measured using a bench top multimeter (Keysight Technologies, 34401A Digital Multimeter, 6½ digit resolution).

In a preliminary test the response of a single sensor was evaluated while temperature was changing rapidly, in a physiological range typically experienced on the surface of the skin. To enable rapid and controlled temperature variation, the sensor was attached onto a hot plate, the temperature control of the plate was switched from Room Temperature to $45\,^{\circ}$C, and as soon as the temperature of the plate reached $32\,^{\circ}$C, plate temperature and RTD resistance were simultaneously recorded every 10 s, in the range between $32\,^{\circ}$C and $42\,^{\circ}$C. This experiment provided the temperature to resistance transfer characteristic reported in part A of Fig. 11, that shows good linearity ($R^2 = 0.99$) and a sensitivity of $0.044\,\Omega/^{\circ}$C.

To investigate variability six different printed sensor specimens were tested in the range of temperatures between $33\,^{\circ}$C and $42\,^{\circ}$C with temperature steps of $1\,^{\circ}$C. At each step, resistance was measured after temperature reached a steady state. All sensors showed a linear characteristic ($R^2 = 0.99$) with average sensitivity, in terms of absolute resistance values, of $0.039 \pm 0.015\ \Omega/^{\circ}$C. Variability observed among sensor units (RSD = $38\,\%$) can be mainly related to process variability that characterizes fast prototyping sensor fabrication, as highlighted in a recent literature review for printed resistive sensors [17], and to some degree of variability in the setup assembly.

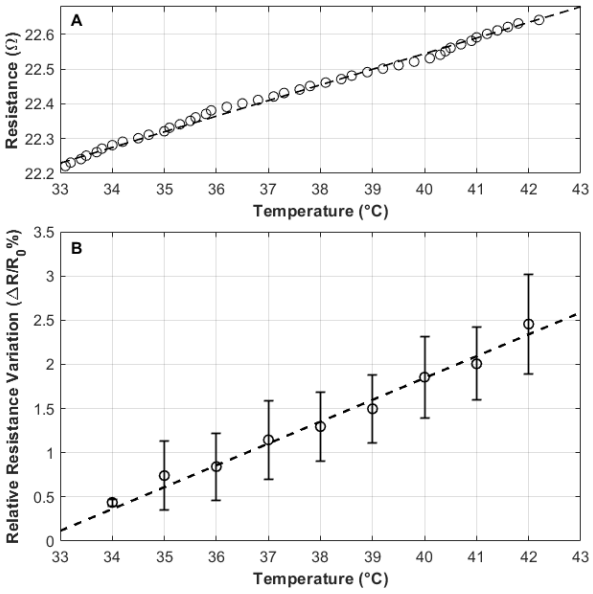

Fig. 11. Response of temperature sensors to temperature variations: A. Response of a single sensor to temperature variation: sample time 10 s, sensitivity $0.044\,\Omega/^{\circ}$C and $R^2 = 0.99$; B. Average transfer characteristic of six sensors to change in steady state temperature: sensitivity of $0.247 \pm 0.056\,\%/^{\circ}$C, TCR of 0.002 and $R^2 = 0.99$

Relative Resistive Variation is plotted in part B of Fig. 11 instead of absolute resistance values, to better highlight the common trend. Here, average sensitivity is $0.247 \pm 0.056\,\%/^{\circ}$C and average RSD is reduced to $22\,\%$. The corresponding value of the Temperature Coefficient of Resistance (TCR) is 0.0025, which appears in agreement with the literature on printed temperature sensors [27].

B. Read-out Circuits

Tests where sensor read-out electronics was included replicated the experiments reported in the previous Section. For BIA electrodes, the same 3D test set-up previously detailed in Sec. IV-A was used, where the human arm is mimicked by a synthetic skin-like patch wrapped around a cylindrical sponge. Controlled hydration levels ranging from $20\,\mu$l/cm^2 to $200\,\mu$l/cm^2 with steps of 10μl/cm^2 were obtained by injecting increasing volumes of deionized (DI) water. After allowing sufficient time to reach a uniform water distribution within the material, the four BIA electrodes in the bracelet were connected to the read-out electronics and impedance values were recorded at a frequency of 1 kHz. These were acquired for 30 s, then averaged to obtain one point in the calibration curve (Fig. 12).

To validate the IE sensor, controlled hydration levels between $10\,\mu$l/cm^2 and $200\,\mu$l/cm^2 were likewise obtained by injecting DI water into the skin-like patch. Impedance was recorded by the two-wire read-out circuit after each injection at a frequency of 100 Hz, at steps of 10μl/cm^2, for 30 s, then averaged to obtain one point in the calibration curve (Fig. 13).

Results obtained in both cases show trends that agree with those obtained during the printed sensors characterization ac-

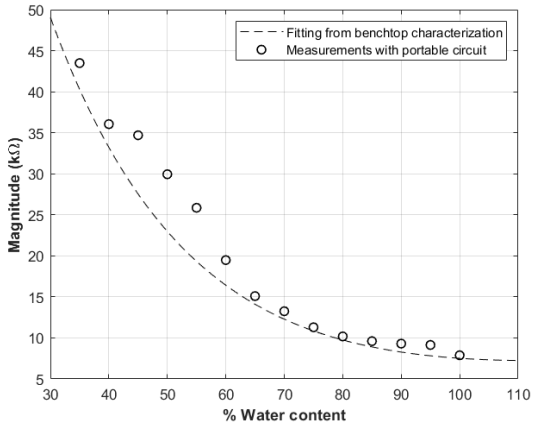

Fig. 12. Response of 4-wire BIA obtained with the portable read-out circuit.

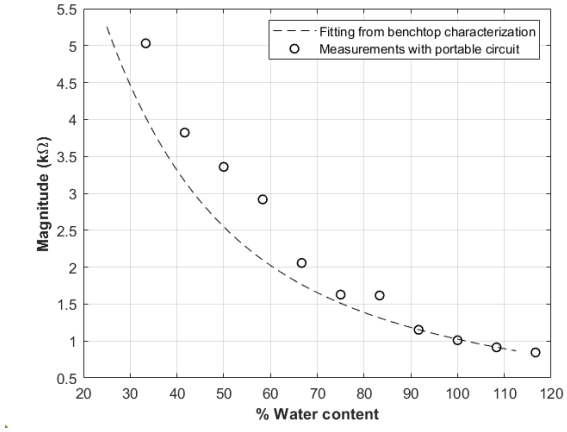

Fig. 13. Response of 2-wire impedance measurement for the skin hydration IE sensor obtained with the portable read-out circuit.

tivity described in Sec. IV-A. As the sensor transfer characteristics are non-linear, higher sensitivities are obtained at lower hydration levels (below $60\,\mu$l/cm^3 for BIA and $60\,\mu$l/cm^2 for skin hydration), whereas saturation can be observed at the higher hydration levels (higher than $160\,\mu$l/cm^3 for BIA and $140\,\mu$l/cm^2 for skin hydration). This means sensitivity gets better when dehydration is approached, which fits with the aims of the system.

The temperature read-out chain for the flexible RTD was calibrated using an ultra-stable PI controller (WTC3243HB, Wavelength Electronics, USA) was acquired and coupled to a thermoelectric cooler (TEC 1.4-6, Thorlabs, USA) and a commercial (TH10K, Thorlabs, USA) negative temperature coefficient thermistor (NTC). The flexible RTD was connected to the read-out chain we developed and placed on the TEC, which is connected to the PI controller and the NTC to complete the control loop. The set temperature of TEC was programmed via the PI controller to step up quickly (in ~ 30 s) from 27 to 45 °C. Then, both the sensed temperature values from RTD front-end and the reading from the commercial NTC were recorded in a triplicated experiment. A very good linear range ($R^2 = 0.9973$) was achieved with sensitivity of $0.0384\Omega/°$C, TCR of 0.00272 and RSD of $12\,\%$ (Fig. 14).

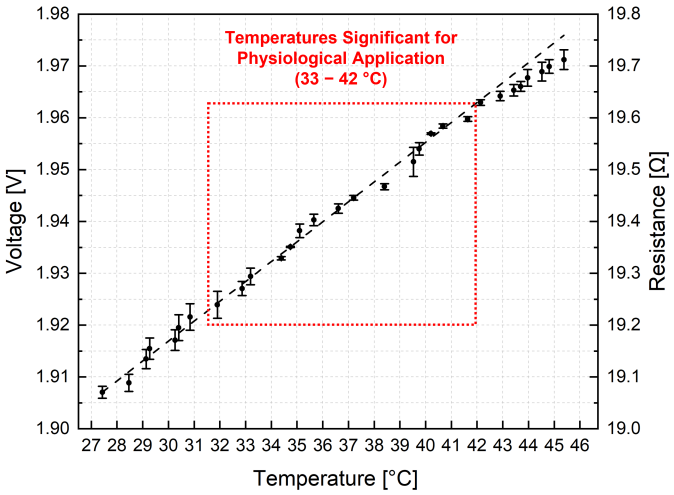

Fig. 14. Response of 4-wire RTD front-end connected to the flexible temperature sensor in dynamic experiment where the temperature changed swiftly from 27 to 45 °C in $\sim$ 30 s. The $R2$ value is 0.9973, sensitivity is $0.0384\,\Omega$/°C, CV is $11.93\,\%$, and three measurements were recorded to compute the error bars.

C. Transmission Validation

System validation was completed by a second test assessing overall system functionality, including the transmitting interface. The test was performed in the laboratory by forwarding the digitized values coming from the read-out electronics during the validation measurement campaign to the network infrastructure. The LoRaWAN gateway is a Dragino LG308, that is a multi-channel gateway capable of receiving and demodulating up to 8 LoRaWAN packets at the same time even if they were broadcast exploiting different SFs on multiple channels. Gateway sensitivity varies depending on the adopted transmission parameters, and in this case (i.e., SF$=$ 7 and bandwidth 125 kHz) it reaches values down to -126 dBm, thus hinting at the long range coverage capability. The gateway is provided with the same type of antenna as the LoRaWAN transceiver of the transmitting interface.

The transmitting interface sampled data with a sampling period of 10 s, then sent information related to the three sensors via LoRaWAN. The network infrastructure on the cloud converted the digitized values into the related sensor measurements. Since the test was carried out in a laboratory, no packet loss occurred. In the light of experience from previous works (e.g., [28]) the same outcome is highly likely also when the receiver is remotely placed (e.g., hospitals). Nonetheless, for this application even a moderate loss of packets can be tolerated, since measured physical quantities are slowly varying over time [29], [30].

Within its application scenario the proposed system will not perform continuous transmission due to two main reasons: (i) targeted parameters are not changing very rapidly over time, thus a transmission period of, e.g., 30 min would be enough; (ii) applications enabled by LoRaWAN protocol must abide by regional regulations related to fair usage of frequency bands [31], limiting temporal occupancy to $1\,\%$ (at least in Europe). An extended interval between transmissions is beneficial from the point of view of power consumption,

translating into an increase of battery lifetime.

The aim of this test was to assess the proper operation of the transmission interface and of the network infrastructure, therefore its duration was only limited to $500\,\mathrm{s}$, transmitting data with an interval of $10\,\mathrm{s}$. Test results confirmed that the transmission interface and the network infrastructure implement transparent transfer of data.

V. Conclusions

The aim of this paper is to propose and characterize *in-vitro* a proof-of-concept prototype of a multi sensing device for monitoring hydration, integrating flexible printed sensors, portable electronics and a LoRaWAN transmitting interface. Characterization of the low-cost printed multi-sensing bracelet showed that each sensor can detect controlled changes of the targeted variable *in-vitro*. Testing performed with the customized electronics showed the ability to reproduce the same experiments performed with bench-top instrumentation, with good accuracy and repeatability. Finally, integration testing of the electronic read-out circuits with the transmission module confirmed the possibility to effectively transmit a package of data from the three sensor every $10\,\mathrm{s}$, which is satisfactory for real-time hydration monitoring.

Results obtained with the prototype discussed in this paper represent a promising start in the development of a fully miniaturized device, to be tested and employed in a real-life application scenario. Future work will focus on *in-vivo* characterization of the printed sensors to test variability and reproducibility, and on the acquisition of different targeted parameters in different hydration conditions.

An essential step to enable a ML-approach will consist of adequately training the algorithm for which gathering a suitable training dataset is necessary. During this phase, the ordinal scale will be employed to associate proper labels to the different hydration levels acquired during *in-vivo* acquisition tests. This will be an essential part since publicly available databases hardly exist and, in any case, they would not be specific to the proposed sensor configuration. The full working prototype here developed will enable the acquisition of reliable and robust training information.

References

[1] A. El-Sharkawy, A. Virdee, A. Wahab, D. Humes, O. Sahota, M. Devonald, and D. Lobo, "Dehydration and clinical outcome in hospitalised older adults: A cohort study," *European Geriatric Medicine*, vol. 8, no. 1, pp. 22–29, 2017.

[2] A. Cataldo, E. De Benedetto, R. Schiavoni, G. Monti, A. Tedesco, A. Masciullo, E. Piuzzi, and L. Tarricone, "Portable Microwave Reflectometry System for Skin Sensing," *IEEE Transactions on Instrumentation and Measurement*, vol. 71, pp. 1–8, 2022.

[3] A. J. Bandodkar, P. Gutruf, J. Choi, K. Lee, Y. Sekine, J. T. Reeder, W. J. Jeang, A. J. Aranyosi, S. P. Lee, J. B. Model, *et al.*, "Battery-free, skin-interfaced microfluidic/electronic systems for simultaneous electrochemical, colorimetric, and volumetric analysis of sweat," *Science advances*, vol. 5, no. 1, p. eaav3294, 2019.

[4] D. Solovei, J. Žák, P. Majzlíková, J. Sedláček, and J. Hubálek, "Chemical sensor platform for non-invasive monitoring of activity and dehydration," *Sensors*, vol. 15, no. 1, pp. 1479–1495, 2015.

[5] H. C. Ates, P. Nguyen, L. Gonzalez-Macia, E. Morales-Narváez, F. Güder, J. Collins, and C. Dincer, "End-to-end design of wearable sensors," *Nature Reviews Materials*, 07 2022.

[6] R. Sokullu, M. A. Akkaş, and E. Demir, "Iot supported smart home for the elderly," *Internet of Things*, vol. 11, p. 100239, 2020.

[7] A. Galli, G. Giorgi, C. Narduzzi, G. Peruzzi, A. Pozzebon, and S. Tonello, "Iot technologies for active ageing: an overview of the elderly dehydration case," in *2022 IEEE International Symposium on Medical Measurements and Applications (MeMeA)*, pp. 1–6, IEEE, 2022.

[8] B. Thomas, B. Cornish, L. Ward, and M. Patterson, "A comparison of segmental and wrist-to-ankle methodologies of bioimpedance analysis," *Applied Radiation and Isotopes*, vol. 49, no. 5, pp. 477–478, 1998. International Symposium on In Vivo Body Comparison Studies.

[9] M. H. Jung, K. Namkoong, Y. Lee, Y. Koh, K. Eom, H. Jang, W. Jung, J. Bae, and J. Park, "Wrist-wearable bioelectrical impedance analyzer with miniature electrodes for daily obesity management," *Scientific Reports*, vol. 11, 01 2021.

[10] M. Usman, A. Gupta, and W. Xue, "Analyzing dry electrodes for wearable bioelectrical impedance analyzers," in *2019 IEEE Signal Processing in Medicine and Biology Symposium (SPMB)*, pp. 1–5, 2019.

[11] S. Abasi, J. Aggas, G. Garayar-Leyva, B. Walther, and A. Guiseppi-Elie, "Bioelectrical impedance spectroscopy for monitoring mammalian cells and tissues under different frequency domains: A review," *ACS Measurement Science Au*, vol. 2, no. 6, pp. 495–516, 2022.

[12] B. Cornish, B. Thomas, and L. Ward, "Effect of temperature and sweating on bioimpedance measurements," *Applied Radiation and Isotopes*, vol. 49, no. 5, pp. 475–476, 1998. International Symposium on In Vivo Body Comparison Studies.

[13] P. Deurenberg, M. Deurenberg-Yap, and F. Schouten, "Validity of total and segmental impedance measurements for prediction of body composition across ethnic population groups," *European Journal of Clinical Nutrition*, vol. 56, no. 3, pp. 214–220, 2002.

[14] F. Sabry, T. Eltaras, W. Labda, F. Hamza, K. Alzoubi, and Q. Malluhi, "Towards on-device dehydration monitoring using machine learning from wearable devices data," *Sensors*, vol. 22, no. 5, 2022.

[15] P. Kassanos, F. Seichepine, and G.-Z. Yang, "A Comparison of Front-End Amplifiers for Tetrapolar Bioimpedance Measurements," *IEEE Transactions on Instrumentation and Measurement*, vol. 70, 2021. Cited by: 2; All Open Access, Hybrid Gold Open Access.

[16] D. Barmpakos and G. Kaltsas, "A review on humidity, temperature and strain printed sensors—current trends and future perspectives," *Sensors*, vol. 21, no. 3, 2021.

[17] P. Bellitti, M. Borghetti, E. Cantù, E. Sardini, and M. Serpelloni, "Resistive sensors for smart objects: Analysis on printing techniques," *IEEE Transactions on Instrumentation and Measurement*, vol. 71, pp. 1–15, 2022.

[18] S. Diaham, "Polyimide in electronics: Applications and processability overview," in *Polyimide for Electronic and Electrical Engineering Applications* (S. Diaham, ed.), ch. 1, Rijeka: IntechOpen, 2021.

[19] R. Harder, A. Diedrich, J. S. Whitfield, M. S. Buchowski, J. B. Pietsch, and F. J. Baudenbacher, "Smart Multi-Frequency Bioelectrical Impedance Spectrometer for BIA and BIVA Applications," *IEEE Transactions on Biomedical Circuits and Systems*, vol. 10, no. 4, pp. 912–919, 2016.

[20] A. Golparvar and M. Yapici, "Toward graphene textiles in wearable eye tracking systems for human-machine interaction," *Beilstein Journal of Nanotechnology*, vol. 12, pp. 180–189, 01 2021.

[21] G. Peruzzi, A. Galli, and A. Pozzebon, "A novel methodology to remotely and early diagnose sleep bruxism by leveraging on audio signals and embedded machine learning," in *2022 IEEE International Symposium on Measurements & Networking (M&N)*, pp. 1–6, IEEE, 2022.

[22] A. Lombardo, S. Parrino, G. Peruzzi, and A. Pozzebon, "Lorawan versus nb-iot: Transmission performance analysis within critical environments," *IEEE Internet of Things Journal*, vol. 9, no. 2, pp. 1068–1081, 2021.

[23] W. C. Chumlea, S. S. Guo, C. M. Zeller, N. V. Reo, and R. M. Siervogel, "Total body water data for white adults 18 to 64 years of age: The fels longitudinal study," *Kidney International*, vol. 56, no. 1, pp. 244–252, 1999.

[24] R. AlDisi, Q. Bader, and A. Bermak, "Hydration assessment using the bio-impedance analysis method," *Sensors*, vol. 22, no. 17, 2022.

[25] S. Ramanathan, M. Jusoh, T. Sabapathy, M. Yasin, S. C. Gopinath, H. ARahim, M. Osman, and Y. A. Wahab, "Elastomeric polydimethylsiloxane polymer on conductive interdigitated electrode for analyzing skin hydration dynamics," *Applied Physics A*, vol. 126, no. 9, pp. 1–11, 2020.

[26] "Hanna instruments, hi 98501 digital thermometer parameters." https://docs.rs-online.com/2c8a/0900766b8136831b.pdf. Accessed: 2023-01-17.

[27] Q. J. Liew, A. S. A. Aziz, H. W. Lee, M. W. Lee, H. F. Hawari, and M. H. Md Khir, "Inkjet-printed flexible temperature sensor based on silver nanoparticles ink," *Engineering Proceedings*, vol. 2, no. 1, 2020.
[28] L. Parri, S. Parrino, G. Peruzzi, and A. Pozzebon, "A LoRaWAN network infrastructure for the remote monitoring of offshore sea farms," in *2020 IEEE International Instrumentation and Measurement Technology Conference (I2MTC)*, pp. 1–6, IEEE, 2020.
[29] G. S. Kelly, "Body temperature variability (part 2): masking influences of body temperature variability and a review of body temperature variability in disease.," *Alternative medicine review*, vol. 12, no. 1, 2007.
[30] H. M. Logan-Sprenger and L. L. Spriet, "The acute effects of fluid intake on urine specific gravity and fluid retention in a mildly dehydrated state," *The Journal of Strength & Conditioning Research*, vol. 27, no. 4, pp. 1002–1008, 2013.
[31] "LoRa Alliance, LoRaWAN 1.0.1 Regional Parameters." https://hz137b.p3cdn1.secureserver.net/wp-content/uploads/2020/11/rp_2-1.0.1.pdf?time=1673563697. Accessed: 2023-01-17.

Sarah Tonello (Member, IEEE) received her M.S. degrees, cum laude, in Biomedical Engineering both from University of Florida and Politecnico di Milano in 2014, as part of the dual degree program Atlantis CRISP. She received the PhD in Technology for Health at the University of Brescia in 2017. During her PhD and Post Doc she has performed several periods abroad as visiting researcher in the Integrated Circuit laboratories of Prof. Sandro Carrara at EPFL, Lausanne. Now she is a researcher in the Department of Information Engineering of the University of Padova. Her research interests include printed sensors, electronic devices and electrochemical sensors.

Alberto Zacchini received his Bachelor's degree in Biomedical Engineering from the University of Padova in 2020 and M.S. degree in Biomedical Engineering from University of Padova in 2023. With a strong academic background and a deep-rooted interest in technology, he's pursuing his career exploring for his own the fascinating intersection of AI and healthcare, specifically focusing on the application of deep learning models in EEG portable devices. He is currently working as Product Specialist at ASA Laser, with key responsibilities related to product development. He is also involved in a Start-up project named MIND AID as a Product Developer of a wearable EEG device.

Alessandra Galli received the B.Sc. and M.Sc. degrees in Biomedical Engineering from the University of Padova, Italy, in 2015 and 2017, respectively. In 2021, she received a Ph.D. degree in Information and Communication Technology from the School of Information Engineering of the University of Padova, with a dissertation about IoT measurements for long-term monitoring applications. In 2021-2022, she was a postdoctoral researcher of the Instrumentation and Measurements Group of the University of Padova, Italy. In September 2023, she joined Eindhoven University of Technology (TU/e) as a postdoctoral researcher supported by a Marie Skłodowska-Curie Postdoctoral fellowship. Her research interests include biomedical signal processing, compression and anomaly detection, and machine learning.

Ata Golparvar (Member, IEEE) received bachelor and master of science in electronics from the Azad University of Tabriz and the Sabanci University of Istanbul in 2016 and 2019, respectively. He is now with the Bio/CMOS Interfaces laboratory in EPFL Neuchatel. His research interests include soft devices and wearable technologies.

Ali Meimandi received B.Sc degree in electrical engineering from Amirkabir University of Technology(Tehran Polytechnic), Tehran, Iran, and M.Sc. degree in electronic engineering from Politecnico di Milano, Milan, Italy, in 2018 and 2022, respectively. He is currently pursuing the Ph.D. degree in the BioCMOS Interfaces(BCI) Laboratory at École Polytechnique Fédérale de Lausanne, Lausanne, Switzerland. His research is focused on designing and implementing ultralow power and Ultralow area analog/mixed-signal IC for brain monitoring. His current research interests include biosensors, neural prosthesis, analog and digital CMOS design, ultra-low-power, and miniaturised CMOS integrated circuits to develop innovative biomedical systems.

Giacomo Peruzzi (Member, IEEE) received the B.Sc. degree in information engineering, the M.Sc. degree in computer and automation engineering, and the PhD in information engineering and science from the University of Siena, Siena, Italy, in 2016, 2019, and 2023 respectively. He is a Research Fellow with the Instrumentation and Measurements Group, University of Padova. His current research interests include in the fields of the Internet of Things (IoT) and distributed measurement systems. In particular, he deals with wireless sensor networks (WSNs) for monitoring systems that are enabled by low-power wide-area network (LPWAN) technologies, as well as embedded machine learning (ML) for measurement infrastructures.

Alessandro Pozzebon (Member, IEEE) received the M.Sc. degree in information engineering, with a focus on the radio frequency identification (RFID) technology applied to cultural heritage, and the Ph.D. degree from the University of Siena, Siena, Italy, in 2006 and 2012, respectively. He is currently an Assistant Professor with the Department of Information Engineering, University of Padova, Padua, Italy, where he teaches with the Laboratory of Electronic Measurements. His main research interests include the development of applications based on low-power wide area network (LPWAN), wireless sensor network (WSN), and RFID technologies in several different application fields, from healthcare to cultural heritage and environmental monitoring.

Nicolò Lago received the bachelor's degree in information engineering, the master's degree in electronic engineering, and the Ph.D. degree in information engineering from the University of Padova, Padua, Italy, in 2012, 2014, and 2017, respectively. His research interests are the characterization and modeling of organic thin-film transistors for biochemical applications, and the modeling and reliability of polymeric and perovskite solar cells for next-generation green electronics. He is currently employed as an electrical technician with Ecoprogetti SRL, Carmignano di Brenta, Italy, working on the research and development of test equipment for solar cells and panels.

Andrea Cester (Senior Member, IEEE) received the M.S. degree in electronic engineering and the Ph.D. degree in electronic and telecommunication engineering from the University of Padua, Padua, Italy, in 1998 and 2002, respectively. He is currently an Associate Professor with the Department of Information Engineering, University of Padova. He is the author/coauthor of more than 200 articles published in international journals and conference proceedings. His research activities range the characterization, reliability study, and modeling of organic electronic devices; photovoltaic devices; graphene-based TFT; and organic biosensors.

Giada Giorgi received the Laurea degree in telecommunications engineering and the Ph.D. degree in microelectronics and telecommunications engineering from the University of Padova, Italy, in 2003 and 2007, respectively. She is currently an Associate Professor with the Department of Information Engineering, University of Padova. Her research activities are in the field of distributed measurement systems and signal processing. They include the development of measurement applications for wireless sensor and actuator networks (WSAN), wireless body sensor networks (WBN), and cyber-physical systems (CPS) and the analysis and development of synchronization algorithms. She is a member of the IEEE TPC-37 (Measurement and Networking).

Sandro Carrara (Fellow, IEEE) is currently a Faculty with EPFL, Lausanne, Switzerland, and a former Professor with the University of Genoa, Genoa, Italy, and the University of Bologna, Bologna, Italy. Along his carrier, he published seven books, with prestigious publishers like Springer/Nature and Cambridge University Press. He has published 400 articles and holds 17 patents. Dr. Carrara was a member of the Board of Governors of the IEEE Circuits and Systems Society (CASS). He is also a member of the Executive Committee of the IEEE Sensors Council. He was a recipient of the IEEE Sensors Council Technical Achievement Award. He is the Editor-in-Chief of the IEEE SENSORS JOURNAL and an Associate Editor of IEEE TRANSACTIONS ON BIOMEDICAL CIRCUITS AND SYSTEMS.

Claudio Narduzzi (Life Member, IEEE) is currently a Full Professor in instrumentation and measurement with the Engineering School, University of Padova, Italy, where he received the Laurea degree in electronics engineering in 1982. His research interests encompass several instrumentation-related application areas in electronics, telecommunications and networking. Current activities are mainly oriented towards networked and IoT-based measurement systems, the analysis of their performances and the application of advanced signal processing methods, such as compressed sensing, in distributed measurement. Prof. Narduzzi is an IEC representative in the JCGM Working Group on the International Vocabulary of Basic and General Terms in Metrology (VIM).